ACOUSTICS 2012

Non-radiative complete SAW bandgap of 2D phononic crystals on semi-infinite LiNbO3 substrate

D. Yudistira[a], Y. Pennec[a], B. Djafari-Rouhani[a], S. Dupont[a] and V. Laude[b]

[a]Institut d'électronique, de microélectronique et de nanotechnologie, avenue Poincaré, Cité scientifique, BP 69, 59652 Villeneuve d'Ascq cedex
[b]Franche-Comté Électronique Mécanique, Thermique et Optique - Sciences et Technologies, 32 avenue de l'Observatoire 25044 Besancon Cedex
d.yudistira@gmail.com

We theoretically demonstrate the existence of complete surface acoustic wave (SAW) bandgap on 2D piezoelectric phononic crystals (PC) consisting of finite air hole arrays with honeycomb arrangement embedded on a semi-infinite YX lithium niobate substrate. Up to now, with a single material structure, complete SAW bandgaps were only demonstrated in the case of a periodic array of pillars on a substrate. The SAW bandgap is determined from PC band structure calculated by means of 3D finite element method (FEM) for which the slowness curve of lithium niobate crystal is incorporated in order to determine the corresponding irreducible Brillouin zone. The effect of hole geometry on the bandgaps has been investigated. We found that, for a given parameter of the air hole, the SAW bandgap is fully situated inside non-radiative region below the sound cone of lithium niobate substrate. SAW transmission through a finite size PC is also presented.

1 Introduction

Phononic crystals (PC) have drawn significant attention since the beginning of 1990's because it offers possibility to control acoustic propagation at wavelength scale thanks to their ability to exhibit phononic (acoustic) bandgap [1,2], range of frequencies that forbid propagation of acoustic waves through the PC structure. Such control has made it possible for interesting physical phenomena in acoustics, such as acoustic waveguides [3], acoustic metamaterials [4], among others, which give rise to several interesting applications such as lab on chip for bio-analysis [5], or phoxonic crystals, when combined with optics or photonic crystals [6]. In some phenomena, i.e. acoustic waveguides, the existence of complete acoustic bandgap determined from the so-called PC band structure, which extends throughout the Brillouin zone, is, in fact, crucial. Of interest to the complete bandgap, many PC configurations have been studied [7,8]. The studies report the existence, for a given well designed phononic crystals structure, of complete acoustic bandgap. Most of the works, however, are mostly focused on the bandgap for bulk phononic crystals or Lamb acoustic waves in periodic plates, for instance drilled with holes [9] or eventually supporting pillars 10. Whereas the non-radiative complete bandgap for surface acoustic waves (SAW), on the other hand, has not attracted as much attention, despite widely use of the SAW in the field of wireless telecommunication. Moreover, the ease of exciting SAW with interdigitated transducers (IDT) or superlattice based transducer [11] on piezoelectric substrate could yield monolithic PC based devices.

First consideration of SAW in semi-infinite two-dimensional (2D) non-piezoelectric PC with circular inclusion has been reported in [12]. Based on a similar configuration, [13] has predicted that a piezoelectric PC with square lattice of semi-infinite air holes on Y-cut $LiNbO_3$ substrate can exhibit full SAW bandgap. The experimental demonstration that followed, however, showed a significant loss in the SAW observed at a frequency above the bandgap [14], which was not predicted by the aforementioned theory. Such losses could be due to the fact the depth of the air hole on the realized PC structure is actually finite. This yields the frequencies above the bandgap lying inside a radiative region within the sound cone of the $LiNbO_3$ substrate defined by the sound line. The sound line is determined from the dispersion relation of the slowest substrate mode. This will, thus, result in the coupling from the SAW to the substrate modes [15]. Apart from some related works presented in [16, 17] with pillars based SAW structure that allows for the existence of complete SAW gap at the frequency far below the sound line as a result of locally resonant mechanism, there is no study about non-radiative complete SAW bandgap on monolithic piezoelectric PC made of finite depth air holes.

In this work, we report on non-radiative complete SAW band gap exhibited by 2D piezoelectric PC made of finite depth air holes on semi-infinite $LiNbO_3$ substrate. The hole constituting the PC is arranged according to a honeycomb lattice. We show that, at a given geometrical parameter of the hole, the SAW bandgap can be well under the sound cone of $LiNbO_3$ substrate and omni-directional gap is obtained.

We initially present the SAW band structures calculated by means of 3D finite element method (FEM). In the simulation, the hole is considered to be finite; unlike the previous study [13], and the slowness curve of the LiNbO3 substrate taking into account piezoelectricity and anisotropy is incorporated in order to determine the corresponding irreducible Brillouin zone. After that, we investigate the effect of geometrical structure of the air hole and subsequent possible imperfection in its shape on the behavior of the SAW bandgap. We finally present the SAW transmission on the finite PC.

2 Model description

Figure 1 (a) shows a top view of a typical 2D PC structure with honeycomb lattice. The corresponding unit cell is illustrated by Fig. 1(b) in a 3D representation. The unit cell, with lattice constant a, includes two identical holes with diameter d and depth h, embedded in a Y-cut $LiNbO_3$ crystal substrate. The crystallographic axes of the substrate are such that Y and Z are aligned with the x_3-axis and the x_2-axis of the PC, respectively. In the finite element model, taking into account the fact that the penetration depth of SAW is roughly one-wavelength from the surface, the thickness of a layer accounting for the substrate was taken to be four times the lattice constant, or 4a. Furthermore, to avoid the excitation of spurious modes under the sound cone, particularly the SAW that may propagate at the free bottom surface of the $LiNbO_3$ layer, an additional $4a$-thick artificial layer with high acoustic velocities when compared with those of $LiNbO_3$ was introduced, as shown in Fig. 1(a). This layer is designed to allow only the excitation of substrate and surface modes within the sound cone of $LiNbO_3$. Owing to the periodicity of the PC, periodic boundary conditions are applied along the x_1 and the x_2 directions. A stress free boundary condition is imposed on the top $+x_3$ surface. Note that the presented results were obtained by considering a stress free boundary condition on the bottom surface. No significant difference was found in the frequency range of interest when the bottom surface was clamped instead. Finally, zero charge electrical boundary conditions are imposed on the top and bottom surfaces.

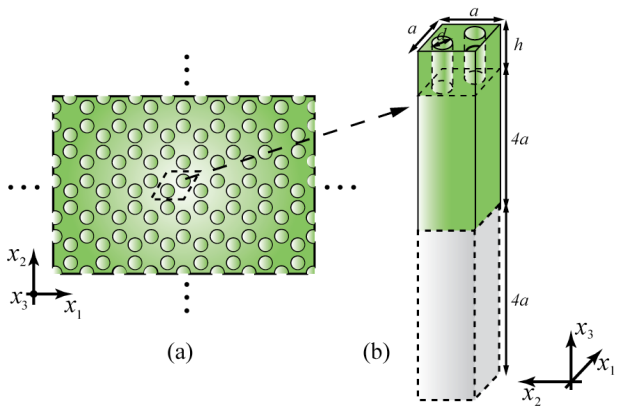

Figure 1: (a) Top view of a 2D piezoelectric PC composed of an air hole array arranged according to a honeycomb lattice. (b) 3D representation of the unit cell where the blue and the grey areas denote the $LiNbO_3$ layer and the artificial layer, respectively.

The governing equations of motion for acoustic waves in $LiNbO_3$, also called electromechanical wave equations, are given by

$$\rho(\mathbf{r})\frac{\partial^2 u_i}{\partial t^2} - c_{ijkl}(\mathbf{r})\frac{\partial^2 u_k}{\partial x_j \partial x_l} - e_{kij}(\mathbf{r})\frac{\partial^2 \phi}{\partial x_k \partial x_j} = 0 \qquad (1)$$

$$e_{ikl}(\mathbf{r})\frac{\partial u_k}{\partial x_i \partial x_l} - \varepsilon_{ik}(\mathbf{r})\frac{\partial^2 \phi}{\partial x_i \partial x_k} = 0$$

with i,j,k and l = 1,2, and 3, and where u is the elastic displacement and ϕ is the electric potential. In Eq. (1), c, e, ε, and ρ are the stiffness tensor, the piezoelectric tensor, the permittivity tensor, and the mass density, respectively. They all depend on position r. Solutions must also satisfy stress free boundary conditions at the interface between $LiNbO_3$ and air holes. Eq. (1) is solved numerically with 3D FEM in conjunction with the boundary conditions described earlier.

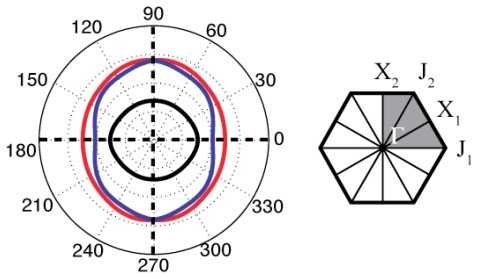

Figure 2: Slowness curves of Y-cut $LiNbO_3$ (*left*) and first Brillouin zone of the honeycomb lattice (*right*). The black, the dark blue and the red lines correspond to the different bulk waves in $LiNbO_3$, while the dashed lines indicate the symmetries of the $LiNbO_3$ crystal. The dark grey area is the first irreducible Brillouin zone with combined material and lattice symmetries.

To calculate the SAW band structure, we firstly determined the irreducible Brillouin zone of the PC. As $LiNbO_3$ is an anisotropic and a piezoelectric crystal, the irreducible Brillouin zone depends not only on the symmetry in the PC lattice as in the case of isotropic PC, but also on the $LiNbO_3$ crystals symmetry, which can be determined from the so-called slowness curve, a plot of the inverse of the acoustic bulk velocities. So by incorporating the symmetry of the slowness curve of the $LiNbO_3$ as shown by the left-hand Fig. 2 to the corresponding Brillouin zone of the PC, which is a hexagonal centered at **K** = 0 with **K** being a wavevector, the corresponding irreducible Brillouin zone can be determined. The zone is, hence, indicated by grey area on the right-hand Fig 2. Once the irreducible Brillouin zone was known, the calculation was performed with **K** taken inside the zone.

3 Results

3.1 Complete SAW bandgaps

The existence of non-radiative SAW complete bandgaps was investigated for two different hole depths: $h = 0.7a$ and $h = 0.9a$. For each depth, the diameter d of the hole was fixed at $0.5a$, the upper limit for a sufficient distance between two adjacent holes for the purpose of technological fabrication.

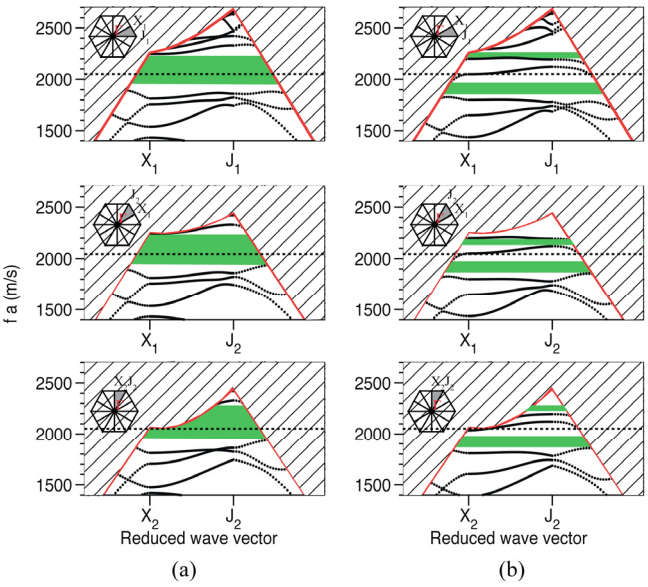

Figure 3: The calculated SAW band structures for the case: $h = 0.7a$, $d = 0.5a$ (a), and $h = 0.9a$, $d = 0.5a$ (b) for the air hole, obtained for each area inside the irreducible Brillouin zone as indicated by the insets. The black dots, red lines, and the patterned areas correspond to the localized SAW modes, the soundline, and the substrates or leaky modes, respectively. The shaded green areas represent the SAW bandgap. The dashed-line represents the frequency of the lowest substrate mode calculated at the zone boundary.

Figure 3 shows the calculated SAW band structure in both cases. In the band structures, black dots identify localized SAW modes that exist below the sound line (i.e., inside the non-radiative region). The sound line is represented with a red color. The region above the sound line (i.e., the sound cone indicated by the patterned area) contains substrate and leaky surface modes that extend both in the PC and in the substrate. The shaded green areas represent the complete SAW bandgaps. Because the sound line limits the (ω,**K**) area that defines non-radiative bandgaps, some bandgaps exist only in a restricted part of

the Brillouin zone, for instance only around point J_2 as is clearly apparent in the last row of Fig. 3. The horizontal dashed line in Fig. 3 is defined by the lowest frequency attained by a bulk wave having its wavevector lying exactly on the Brillouin zone boundary. SAW bandgaps below this dashed-line are omnidirectional since they extend in all propagation directions. It can be seen that such an omnidirectional bandgap exists for both considered values of the depth of the holes.

3.2 Effect of hole geometry on the SAW bandgap

To further investigate the effect of geometrical structure of the hole on the SAW bandgap, the above calculation was repeated with the depth h and the diameter d of the hole being taken as a parameter. The SAW gap maps were generated, which are shown in Figs. 4. Figure 4(a) corresponds to the gap map for the case when the diameter d was kept constant at $d = 0.5a$ and the depth h was constantly increased from $0.5a$ to $1a$. And Fig. 4(b) shows the gap map for the case of the depth h fixed at $h = 0.9a$ and the diameter d was increased from $0.35a$ to $0.5a$. The case of $h > 1a$ was not considered because in general the depth of the holes in the technological fabrication does not go much beyond this range while we demonstrate the possibility of complete SAW bandgap for $h < 1a$.

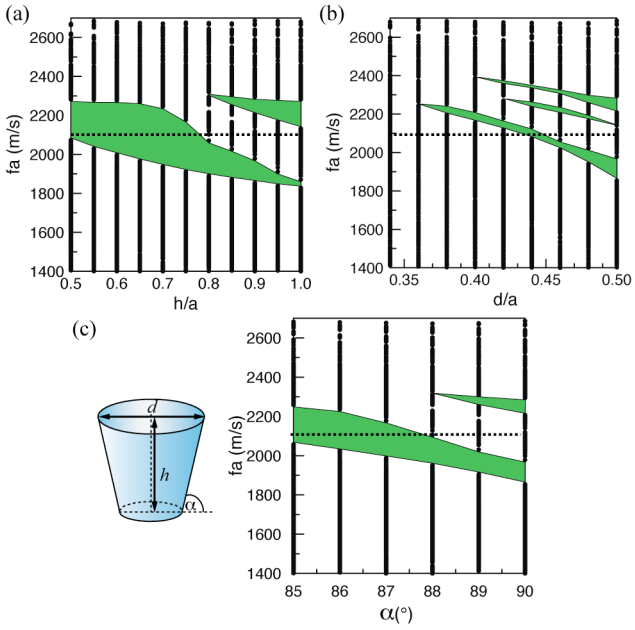

Figure. 4: Calculated SAW gap maps for the case when the depth h is varied from $5a$ to $1a$ while the diameter d is fixed at $d = 0.5a$ (a), and when the diameter d is varied from $0.34a$ to $0.5a$ while the depth h is fixed at $h = 0.9a$ (b). (c) Calculated SAW gap map for the case when the shape of the hole is changing from conical to cylindrical by varying angle α from 85° to 90°, with $h = 0.9a$ and $d = 0.5a$. The inset illustrates the shape of the conical hole.

Figure 4(a) shows from $h = 0.5a$ to about $h = 0.7a$ the gap is widening and after that from $h = 0.7a$ to $h = 1a$ the gap is narrowing and shifting downward to the lower frequency towards the case of a semi-infinite PC, while at the same time higher frequency gap appears from $h = 0.85a$ to $h = 1a$. We can see that with respect to the dashed-line explained before, at $h = 0.5a$ and $h < 0.5a$ (if the gap exists) the lower gap along with the upper gap ($h = 0.85a$ to $h = 1a$) appears only above the line, which, hence, exists in some particular directions of the Brillouin zone as previously explained. However, from $h = 0.55a$ to $h = 1a$ the omni-directional gap is emerging on the lower gap. Following is when d was varied with h being fixed at $0.9a$, we find three bandgaps with the maximum width of the gap obtained from the lower gap at $d = 0.5a$ as shown in Fig. 4(b). We also see that when the diameter d is increased, all the gaps are shifting downward to the lower frequency and widening at the same time, except the middle gap that vanishes when $d = 0.48a$. In addition to that with respect to the dashed-line, all gaps, except the lower one, only exist in particular directions whereas from $d = 0.44a$ to $d = 0.5a$ the omni-directional gap is obtained from the lower gap.

Until now the hole constituting the PC structure is considered to be in cylindrical shape. However, in reality, due to fabrication imperfections, the hole is more likely to be in a conical shape [15] with a slope angle α as shown by the inset of Fig. 4(c), which will affect the bandgap. To investigate the effect of the hole shape, here, we took α as a variable with α being varied from 85° to 90°. When α = 90° the cylindrical hole is obtained as previously considered. For each value of α, the depth h and the diameter d of the hole were fixed at 0.9a and 0.5a, respectively, taken from the structure considered previously. The calculated gap map is given in Fig. 4(c), which shows when the shape of the hole changes from conical to cylindrical, the gap is shifting downward to the lower frequency and the higher gap emerges after 88°. Apart from that the omni-directional gap emerges after α = 85° from the lower gap and it is completely below the dashed-line after α = 88°. The upper gap lies above the dashed-line therefore will only exist in some particular directions.

3.3 SAW transmission on finite size of PC

Figure 5(a) shows 3D model structure of a finite PC for the transmission analysis. Here, a PC of $h = 0.85a$ and $d = 0.5a$ was considered consisting of 9 columns and 5 rows. The SAW source is placed for about few lambdas away from the PC and excites SAW propagating along x_1 direction parallel to Γ-J_1. Three points were considered A (lower pass band), B (inside the lower bandgap) and C (upper pas band), which are situated at a different position on the band structure in Fig. 5(b). Figure 6 shows the SAW transmission calculated at each point, which is in a good agreement with the calculated band structure.

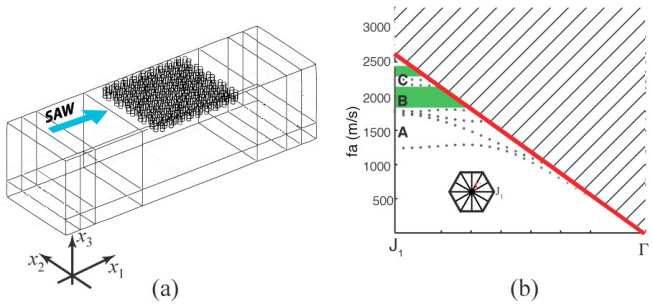

Figure. 5: (a) 3D model of finite PC structure being considered for transmission analysis. (b) Band structure in

Γ-J_1 direction calculated from a PC of h = 0.85a and d = 0.5a.

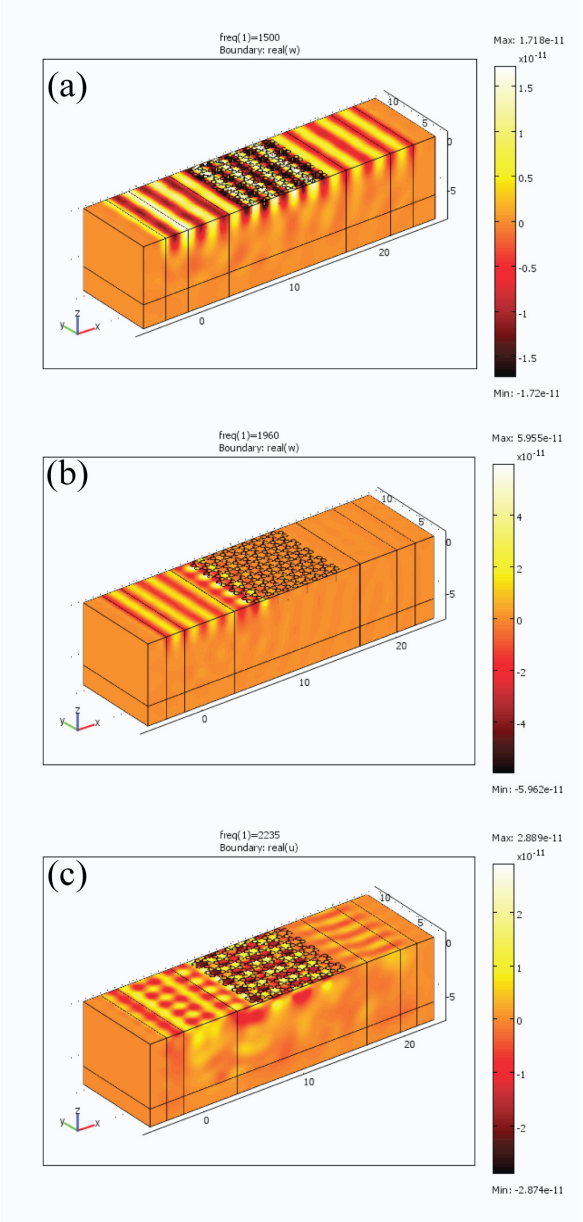

Figure. 6: Out-of-plane displacement component of the SAW propagating along x_1 direction into a finite PC calculated at point A (a), B (b), and C (c).

5 Conclusion

As a conclusion, we have identified non-radiative complete SAW bandgaps for monolithic piezoelectric phononic crystals composed of finite-depth air holes arrays arranged according to a honeycomb lattice on a semi-infinite $LiNbO_3$ substrate. Bandgaps were determined from the SAW band structure calculated using 3D FEM, with the anisotropy and piezoelectricity of $LiNbO_3$ included in the definition of the relevant irreducible Brillouin zone. The non-radiative bandgaps that are obtained are located under the sound cone of the $LiNbO_3$ substrate. In addition to omnidirectional bandgaps, directional bandgaps are found as well for given parameters and shapes of the hole. We have also presented the simulation of the SAW transmission through a finite size of the PC, which shows a good agreement with the band structure results.

Acknowledgments

This work is founded by ANR (P3N2009) within Project No. ANR-09-NANO-004 (phoXcry).

References

[1] M.S. Kushwaha, P. Halevi, L. Dobrzynski, and B. Djafari-Rouhani, *Phys. Rev. Lett.* 71, 2022 (1993)

[2] M. Sigalas and E.N. Economou, *Solid State Commun.* 86, 141 (1993)

[3] J. Hwan Oh, I. Kyu Lee, P. Sik Ma, and Y. Young Kim, *Appl. Phys. Lett.* 99, 083505 (2011)

[4] N. Fang, D. Xi, J. Xu, M. Ambati, W. Srituravanich, C. Sun, and X. Zhang, *Nat. Mater.* 5, 452 (2006)

[5] R. Wilson, J. Reboud, Y. Bourquin, S.L. Neale, Y. Zhang, and J.M. Cooper, *Lab Chip* 11, 323 (2010)

[6] M. Maldovan and E.L. Thomas, *Appl. Phys. Lett.* 88, 251907 (2006)

[7] S. Sadat-Saleh, S. Benchabane, F.I. Baida, M.-P. Bernal, and V. Laude, *J. Appl. Phys.* 106, 074912 (2009)

[8] Y. Pennec, B.D. Rouhani, E.H. El Boudouti, C. Li, Y. El Hassouani, J.O. Vasseur, N. Papanikolaou, S. Benchabane, V. Laude, and A. Martinez, *Opt. Express* 18, 14301 (2010)

[9] S. Mohammadi, A.A. Eftekhar, A. Khelif, H. Moubchir, R. Westafer, W.D. Hunt, and A. Adibi, *Electron. Lett.* 43, 898 (2007)

[10] Y. Pennec, B. Djafari Rouhani, H. Larabi, A. Akjouj, J.N. Gillet, J.O. Vasseur, and G. Thabet, *Phys. Rev. B* 80, 144302 (2009)

[11] D. Yudistira, S. Benchabane, D. Janner, and V. Pruneri, *Appl. Phys. Lett.* 95, 052901 (2009)

[12] Y. Tanaka and S. Tamura, *Phys. Rev. B* 58, 7958 (1998)

[13] V. Laude, M. Wilm, S. Benchabane, and A. Khelif, *Phys. Rev. E* 71, 036607 (2005)

[14] S. Benchabane, A. Khelif, J.-Y. Rauch, L. Robert, and V. Laude, *Phys. Rev. E* 73, 065601 (2006)

[15] A. Khelif, Y. Achaoui, S. Benchabane, V. Laude, and A. Boujemaa, *Phys. Rev. B* 81, 214303 (2010)

[16] M. B. Assouar, and M. Oudich, *Appl. Phys. Lett.* 99, 123505 (2011)